AGU PUBLICATIONS

Global Biogeochemical Cycles

RESEARCH ARTICLE
10.1002/2015GB005302

Key Points:
- Topographic heterogeneity drives the spatiotemporal variation in erosion and fate of soil organic C
- Episodic representation of C erosion and burial improves prediction of C fluxes
- Small-scale complexity of C erosion leads to strong topographic variability of dynamic C replacement

Supporting Information:
- Supporting Information S1

Correspondence to:
Y. G. Dialynas,
ydialynas@gatech.edu

Citation:
Dialynas, Y. G., S. Bastola, R. L. Bras, S. A. Billings, D. Markewitz, and D. d B. Richter (2016), Topographic variability and the influence of soil erosion on the carbon cycle, *Global Biogeochem. Cycles*, *30*, 644–660, doi:10.1002/2015GB005302.

Received 2 OCT 2015
Accepted 20 APR 2016
Accepted article online 22 APR 2016
Published online 11 MAY 2016

Topographic variability and the influence of soil erosion on the carbon cycle

Yannis G. Dialynas[1], Satish Bastola[1], Rafael L. Bras[2], Sharon A. Billings[3], Daniel Markewitz[4], and Daniel deB. Richter[5]

[1]School of Civil and Environmental Engineering, Georgia Institute of Technology, Atlanta, Georgia, USA, [2]School of Civil and Environmental Engineering and School of Earth and Atmospheric Sciences, Georgia Institute of Technology, Atlanta, Georgia, USA, [3]Department of Ecology and Evolutionary Biology and Kansas Biological Survey, University of Kansas, Lawrence, Kansas, USA, [4]Warnell School of Forest Resources, University of Georgia, Athens, Georgia, USA, [5]Nicholas School of the Environment and Earth Sciences, Duke University, Durham, North Carolina, USA

Abstract Soil erosion, particularly that caused by agriculture, is closely linked to the global carbon (C) cycle. There is a wide range of contrasting global estimates of how erosion alters soil-atmosphere C exchange. This can be partly attributed to limited understanding of how geomorphology, topography, and management practices affect erosion and oxidation of soil organic C (SOC). This work presents a physically based approach that stresses the heterogeneity at fine spatial scales of SOC erosion, SOC burial, and associated soil-atmosphere C fluxes. The Holcombe's Branch watershed, part of the Calhoun Critical Zone Observatory in South Carolina, USA, is the case study used. The site has experienced some of the most serious agricultural soil erosion in North America. We use SOC content measurements from contrasting soil profiles and estimates of SOC oxidation rates at multiple soil depths. The methodology was implemented in the tRIBS-ECO (Triangulated Irregular Network-based Real-time Integrated Basin Simulator-Erosion and Carbon Oxidation), a spatially and depth-explicit model of SOC dynamics built within an existing coupled physically based hydro-geomorphic model. According to observations from multiple soil profiles, about 32% of the original SOC content has been eroded in the study area. The results indicate that C erosion and its replacement exhibit significant topographic variation at relatively small scales (tens of meters). The episodic representation of SOC erosion reproduces the history of SOC erosion better than models that use an assumption of constant erosion in space and time. The net atmospheric C exchange at the study site is estimated to range from a maximum source of 14.5 g m^{-2} yr^{-1} to a maximum sink of −18.2 g m^{-2} yr^{-1}. The small-scale complexity of C erosion and burial driven by topography exerts a strong control on the landscape's capacity to serve as a C source or a sink.

1. Introduction

Accelerated soil erosion redistributes soil organic carbon (C) across the landscape with significant impacts on the soil-atmosphere C exchange. Assessing the role of erosion and deposition on the C cycle is critical not only for understanding future challenges posed by climate change but also for providing strategies for climate change mitigation [*Battin et al*., 2009; *Lal*, 2004]. Stallard [1998] first pointed out that erosion and deposition may explain a significant portion of the so-called "missing sink" [*Lal*, 2003, 2004; *Liu et al*., 2003] in atmospheric CO_2. Global assessments on the net effect of soil erosion on the C cycle are currently based on significantly different assumptions about the associated operating processes [*Harden et al*., 1999; *Jacinthe and Lal*, 2001; *Lal*, 2003; 2004; *Regnier et al*., 2013; *Smith et al*., 2001; *Stallard*, 1998; *Van Oost et al*., 2012; *Van Oost et al*., 2007]. Depending on assumptions, estimates of erosion's impact on the global C cycle range from a C sink exceeding −1 Pg yr^{-1} [*Harden et al*., 1999; *Stallard*, 1998] to a C source of around 1 Pg yr^{-1} [*Jacinthe and Lal*, 2001; *Lal*, 2004].

A key feature driving differences among these estimates is the notable absence of knowledge about the fate of eroded soil organic C (SOC). Multiple studies implicitly invoke assumptions about that fate [*Lal*, 1995; *Smith et al*., 2001] or explicitly assess how assumptions about the fate of eroded SOC influence soil-atmosphere C flux estimates [*Billings et al*., 2010]. In extreme scenarios eroded SOC is either fully protected from oxidation [*Smith et al*., 2001], or is oxidized to its entirety [*Lal*, 1995], leading to a range of possible net soil-atmosphere C flux estimates. The net effects of erosion and deposition on the C exchange between terrestrial ecosystems and the atmosphere continue to be studied [*Billings et al*., 2010; *Van Oost et al*., 2007], and the potential of

coupled spatially explicit, physically based models that account for the fate of eroded C has been widely recognized [*Hu and Kuhn*, 2014; *Liu et al*., 2003].

Globally, soils affected by human interventions are dynamic, rapidly changing systems [*Doetterl et al*., 2012; *Richter and Markewitz*, 2001] impacted by many processes, the interrelations of which are still poorly understood [*Van Oost et al*., 2007]. SOC storage models of eroding soils that have recently been proposed in the literature [*Billings et al*., 2010; *Coleman et al*., 1997; *Harden et al*., 1999; *Liu et al*., 2003; *Rosenbloom et al*., 2006; *Stallard*, 1998; *Van Oost et al*., 2005, 2012; *Yoo et al*., 2005] are based on conceptual formulations of underlying natural mechanisms and involve limited linkages among fundamental processes. Accounting for dynamic feedback among the complex physical, chemical, and biological processes driving SOC fluxes can be crucial when evaluating soil-atmosphere C exchange [*Liu et al*., 2003; *Van Oost et al*., 2007]. Also important is the representation of land management practices [*Dlugoß et al*., 2012; *Hu and Kuhn*, 2014], such as enhancement or degradation of system productivity. Management practices may regulate the extent to which SOC oxidation and production, important components of the soil-atmosphere CO_2 exchange, are altered by erosion [*Billings et al*., 2010]. The effect of management practices on SOC redistribution via erosion and deposition in complex topographies remains poorly investigated.

This work proposes a novel approach to assess the impact of episodic erosion on atmospheric CO_2 by systematically accounting for dynamic feedback among coupled hydrological, geomorphological, and biogeochemical processes in a physically based, spatially explicit framework and utilizing measurements of depth-dependent biogeochemical properties [*Billings et al*., 2010; *Richter et al*., 1999]. The work emphasizes the dynamic interaction between eroding and depositional sites on the redistribution of SOC at daily time scales. We estimate the fate of eroded SOC across a topographically heterogeneous landscape, and we explore the role of management practices on the C exchange with the atmosphere.

2. Methods

2.1. Spatially Explicit Biogeochemical Model

To quantify the influence of C erosion and deposition on atmospheric CO_2 we introduce tRIBS-ECO (Triangulated Irregular Network-based Real-time Integrated Basin Simulator-Erosion and Carbon Oxidation) [*Dialynas et al*., 2014], a spatially explicit model of SOC dynamics developed within the existing coupled physically based hydro-geomorphic model [*Francipane et al*., 2012] discussed in section 2.2. The model incorporates a SOC mass balance equation for each computational cell. Continuous functions of depth-dependent quantities representing SOC storage and C fluxes with the atmosphere, including SOC production and oxidation losses are used, in addition to lateral SOC fluxes due to soil erosion and deposition. Depth-dependent variables are integrated over soil thickness, which constitutes a temporally variant boundary condition, as it is locally controlled by episodic erosion and deposition. For each cell and at each time step the SOC mass balance equation (for a unit area) is

$$\frac{\Delta \mathrm{SOC}}{\Delta t} = \int_0^{H_t} I_t(z)dz - \int_0^{H_t} k_t(z)\rho(z)C_t(z)dz - \frac{1}{\Delta t}\int_0^{h_t}\rho(z)C_t(z)dz\Big|_{\mathrm{out}} + \frac{1}{\Delta t}\sum_{i=1}^{n}\int_0^{h_{t,i}}\rho_i(z)C_{t,i}(z)dz\Big|_{\mathrm{in}} \quad (1)$$

where the subscript t is time step (T), z is depth (L), H_t is time-varying soil thickness (L), SOC is total soil organic C storage in the soil column (ML^{-2}), $I_t(z)$ is SOC production ($\mathrm{ML}^{-3}\,T^{-1}$), $k_t(z)$ is SOC decomposition rate constant (T^{-1}), $\rho(z)$ is bulk density (ML^{-3}), $C_t(z)$ is SOC mass fraction (MM^{-1}), h_t is the eroded soil layer (L) estimated by the geomorphic model, and n is the number of upstream cells contributing to lateral SOC influx. Exponential functions were used [*Ni et al*., 2012; *Rosenbloom et al*., 2006; *Yoo et al*., 2005] to parsimoniously represent the depth-dependent SOC production and decomposition rates and SOC content (section 4.1). The sum of the first two terms of the right-hand side of equation (1) represents the net C flux between soil and the atmosphere. The third and fourth terms are SOC loss due to erosion and lateral SOC influx from upstream cells, respectively.

In tRIBS-ECO the watershed's hydro-geomorphic response to hydrometeorological forcings leads to spatially heterogeneous, episodic erosion. Equation (1) is applied with a daily time resolution to systematically account for the fate of eroded SOC in a network of computational elements. Eroded SOC can be oxidized upon transport, or it can be stored at deeper horizons at depositional sites, where oxidation is mitigated.

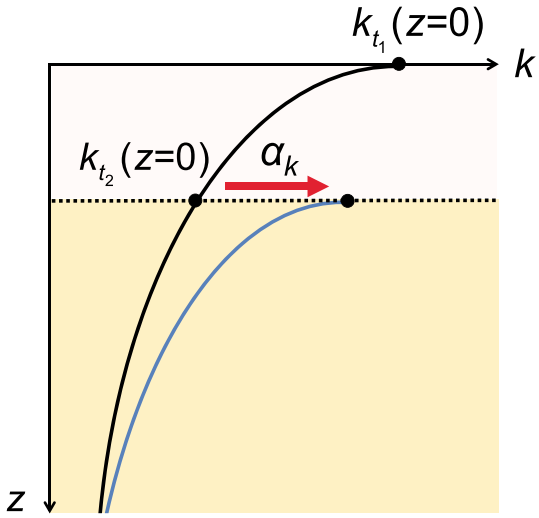

Figure 1. Illustration of the effect of management practices on altered depth-dependent SOC oxidation $k_t(z)$. Assume that by time t_2 soil erosion leads to the removal of a soil layer with the new surface having an oxidation rate $k_{t_2}(z = 0)$, altered from $k_{t_1}(z = 0)$. We propose that land management practices can have an effect on altered oxidation at a rate a_k (see section 2.1). The framework is also applied to SOC production [*Billings et al.*, 2010].

The proposed framework quantifies the watershed-integrated net contribution to atmospheric CO_2 derived from erosional processes.

The influence of land management practices on altered SOC oxidation and production rates by erosion is also considered. Severe erosion events can significantly alter the depth-dependent SOC oxidation and production at disturbed sites by the lateral removal of topsoil. However, this can be moderated by management practices, which alter SOC oxidation and production over surficial and deeper horizons [*Billings et al.*, 2010]. We introduce coefficients a_k and a_I, corresponding to the influence of management practices on altered SOC oxidation and production rates, respectively. To clarify this framework an example is given in Figure 1. Assume that by time t_2 removal of an eroding soil layer leads to the new surface having an oxidation rate $k_{t_2}(z = 0)$, which can be significantly different from the original rate, $k_{t_1}(z = 0)$ [*Billings et al.*, 2010]. Management practices restore the initial $k_{t_1}(z)$ at a rate specified by the coefficient a_k. This framework is also applied to the depth-dependent SOC production. Moreover, a_I and a_k are applied with no reference to ongoing erosion rate. Thus, the effect of management practices on disturbed profiles is represented even for periods characterized by low erosion rates.

The proposed spatially and depth-explicit approach has important advantages and novel features over existing efforts (e.g., [*Billings et al.*, 2010; *Rosenbloom et al.*, 2006; *Yoo et al.*, 2005]) that attempt to describe erosion effects on soil-atmosphere C exchange. Advances of the proposed physically based framework include the coupling of hydrologic, geomorphic, and biogeochemical processes at the watershed scale; leading to an episodic representation of SOC erosion; tracking the potential of eroded SOC to undergo mineralization or be stabilized based on local topographic variation; and dynamically representing the effect of land management practices on altered SOC oxidation and production at eroding sites.

2.2. Physically Based Representation of Hydrological and Geomorphological Processes

tRIBS (Triangulated Irregular Network (TIN)-based Real-time Integrated Basin Simulator) is the underlying hydrologic model [*Ivanov et al.*, 2004a, 2004b; *Vivoni et al.*, 2004]. tRIBS explicitly accounts for the spatial variability of precipitation fields and land-surface descriptors. It represents soil moisture dynamics and stresses the role of topography in lateral soil moisture redistribution by accounting for the effects of heterogeneous and anisotropic soil. The computational elements of the model are Voronoi polygons defined by the TIN network. The geometry and properties of the Voronoi polygons are described in *Vivoni et al.* [2004]. The basin's hydrologic response can be simulated at very fine temporal (hourly) and spatial (10 to 100 m) scales. Modeled hydrological processes include runoff routing, rainfall canopy interception, evapotranspiration, and surface energy balance, infiltration, and lateral redistribution of soil moisture in the unsaturated and saturated zones. The underlying hydrological processes are described by a set of physically based formulations. The model accounts for different soil types and vegetation species in representing hydrological processes in a spatially explicit, physically based manner.

Infiltration is modeled by assuming gravity-dominated flow in heterogeneous, anisotropic soil [*Garrote and Bras*, 1995]. In each computational element, the evolution of a wetting front and a top front may lead to unsaturated, perched-, surface-, or completely saturated states. The unsaturated and saturated zones are coupled to account for the interaction of the dynamic groundwater table with the moving wetting front. Lateral moisture transfer in the unsaturated zone is controlled by topography, while continuous soil moisture allows for redistribution during both storm and interstorm periods, which allows long-term simulations over a range of hydrometeorological forcings. Groundwater flow is represented by means of a quasi three-dimentional

"cascade" model. The groundwater model allows for lateral redistribution in the saturated zone, in addition to dynamic interaction with the unsaturated zone. Surface runoff is generated by different mechanisms, as a result of the dynamic interaction of lateral soil moisture redistribution, infiltration fronts, and water table depth. Saturation excess, infiltration excess, perched subsurface stormflow, and groundwater exfiltration are the four runoff-generating mechanisms in the model.

tRIBS was coupled with a geomorphic model (tRIBS-Erosion [*Francipane et al*., 2012]), which is based on the Channel-Hillslope Integrated Landscape Development model [*Tucker et al*., 2001a, 2001b]. The model simulates the main erosive processes on hillslopes and in channels, including raindrop impact detachment and overland flow entrainment, in addition to diffusive processes. Sediment discharge and changes in elevation are computed at each computational element. Soil erosion and deposition dynamically feedback to the hydrology through local changes in topographic characteristics and drainage network configuration, which highlights the coupled character of the hydro-geomorphic model. Elevation differences from soil erosion and deposition lead to topography that evolves in time.

The hydro-geomorphic model represents rain splash erosion, which is an important erosion-inducing mechanism on interfluves and hillslopes. Raindrop impact destroys soil aggregates, enabling the initiation of sediment motion. The model includes different factors that control raindrop impact detachment, such as rainfall characteristics, soil type, ground and canopy cover, and depth of overland flow. Subgrid spatial variability within the Voronoi cells is accounted for through areal fractions of features such as vegetation, and bare soil, as well as variability of processes like throughfall. Both the effects of direct rain splash detachment and leaf drip are accounted for. The model also accounts for soil erosion and deposition by overland flow at hillslopes and channels. Shear stress-based formulations for sediment initiation of motion, entrainment, and transport capacity by surface runoff are also represented. Raindrop erosion and overland flow erosion are represented by physically based and by empirical relations. The geomorphic model estimates entrainment-limited and transport-limited sediment discharges at each computational unit. The final erosion potential at each time step is estimated by accounting for the transport capacity, flow entrainment capacity, and topographic gradients at each Voronoi cell. Local elevation change at eroding and depositional sites is computed, and terrain characteristics are subsequently updated, which feedback to hydrologic and erosional dynamics.

2.3. Soil Organic Carbon, Erosion, Replacement, and Oxidation Model

The SOrCERO (Soil Organic Carbon, Erosion, Replacement, and Oxidation) model was introduced by *Billings et al*. [2010]. The depth-explicit model quantifies the effect of constant erosion and altered SOC production and oxidation on CO_2 release to the atmosphere at a single eroding soil profile. Model inputs include an assumed constant erosion rate, depth-dependent SOC content, oxidation, and production rates. The moderating effect of management practices on erosion driven C fluxes is explicitly considered. More precisely, the mixing coefficients n_{ox} and n_{prod} express the extent to which erosion alters SOC oxidation and production rates at the eroding site. Outputs include SOC storage and eroded SOC, and maximum C sink or source strengths depending on the amount of eroded SOC assumed to be oxidized.

3. Study Area

We assess the watershed-integrated hydro-geomorphic response of the 4.3 km^2 Holcombe's Branch watershed (34.6177°N, 81.6914°W; Figure 2a) in terms of SOC redistribution and atmospheric CO_2 flux. The Holcombe's Branch is a tributary of the Tyger River, which drains into the Broad, Congaree, and Santee Rivers before entering the Atlantic Ocean. The watershed is part of the Calhoun Critical Zone Observatory and U.S. Department of Agriculture Forest Service Calhoun Experimental Forest in the Piedmont of South Carolina, USA. The region has experienced some of the most serious agricultural land degradation in North America [*Trimble*, 1974]. The mean annual precipitation is around 1260 mm, and the mean annual temperature is about 17°C. Elevation ranges from 113 m to 196 m above sea level. The watershed is covered for the most part by highly weathered acidic Ultisol and Inceptisol soils [*Richter and Markewitz*, 2001; *Richter et al*., 2014]. The soil and vegetation types characterizing the study area are discussed in section 4. Cultivation of cotton, corn, wheat, and other crops led to significant soil erosion starting about 1800 and continuing to the early twentieth century [*Richter and Markewitz*, 2001]. The Calhoun Experimental Forest includes one of the longest running experiments on soil properties and processes worldwide [*Richter et al*., 1999], providing insights that support this study [*Richter and Markewitz*, 2001; *Richter et al*., 2006].

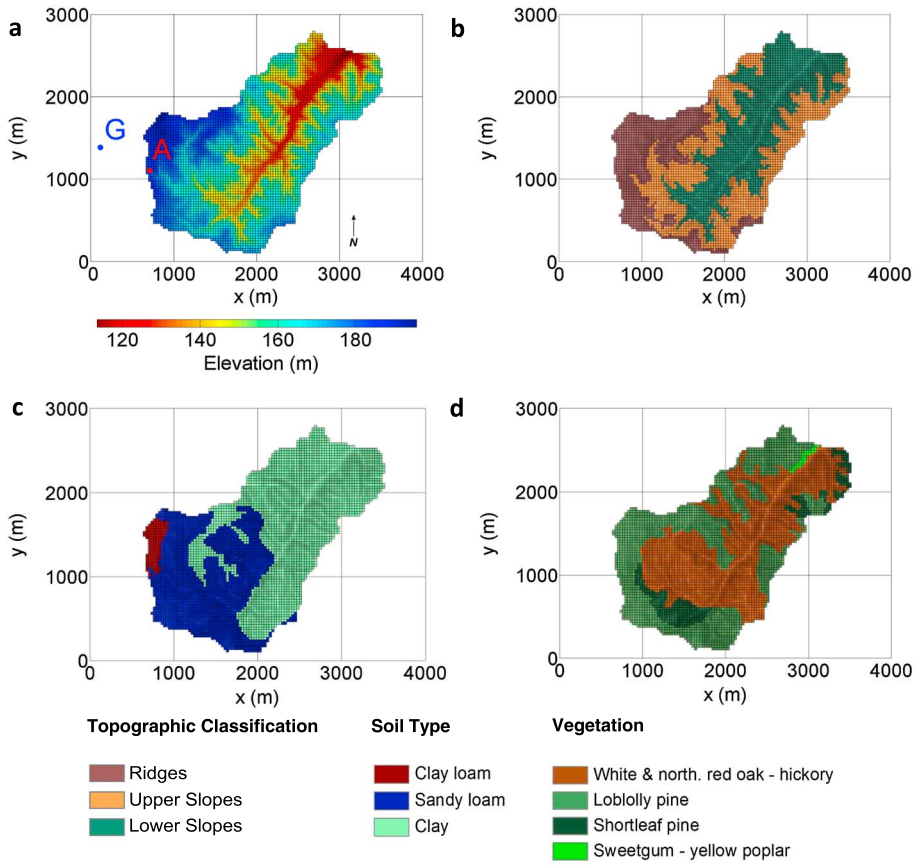

Figure 2. (a) Digital elevation model of the Holcombe's Branch watershed; sites A and G are illustrated by red and blue points, respectively; (b) topographic classification of the watershed; initial total SOC storage (calculated in the upper 5 m of soil) at ridges, upper, and lower slopes is equal to 10.3 kg m^{-2}, 12.7 kg m^{-2}, and 16.7 kg m^{-2}, respectively; (c) spatial distribution of soil textural classes; and of (d) vegetation types.

4. Model Input Data and Parameters

The biogeochemical, topographic, hydrological, and geomorphic input data and parameters necessary for tRIBS-ECO are summarized in the following sections, in addition to initialization and validation procedures. Additional information is provided in the supporting information.

4.1. Biogeochemical Parameters

Biogeochemical input variables to tRIBS-ECO were obtained from a relatively undisturbed soil profile in a hardwood stand nearby (site G in Figure 2a), which is considered to have never been cultivated [*Billings et al.*, 2010; *Richter and Markewitz*, 2001]. Distributions with depth of SOC content and bulk density were obtained from previous studies at the site [*Billings et al.*, 2010; *Markewitz and Richter*, 1998; *Richter et al.*, 1999]. First-order mean oxidation rate constants (k, yr^{-1}) for the undisturbed soil profile [*Billings et al.*, 2010] were estimated from mean residence times calculated using bulk radiocarbon signatures of organic C from several soil horizons sampled in 1962 [*Richter et al.*, 1999], likely before the presence of thermonuclear bomb-produced ^{14}C [*Billings et al.*, 2010; *Richter et al.*, 1999]. The corresponding input parameters to tRIBS-ECO were estimated by fitting the following exponential functions with depth to the associated data, by means of constrained nonlinear optimization (see Figure 3):

$$C_t(z) = C_{a,t}e^{C_{b}z} + C_c \tag{2}$$

$$k_t(z) = k_{a,t}e^{k_{b}z} + k_c \tag{3}$$

$$\rho(z) = \rho_a e^{\rho_{b}z} + \rho_c e^{\rho_{d}z} + \rho_e e^{\rho_{f}z} \tag{4}$$

for SOC content, oxidation rate, and soil bulk density, respectively (see section 2.1 for notation). Equations (2) and (3) correspond to dynamic exponential profiles of SOC content and of SOC decomposition rate (see

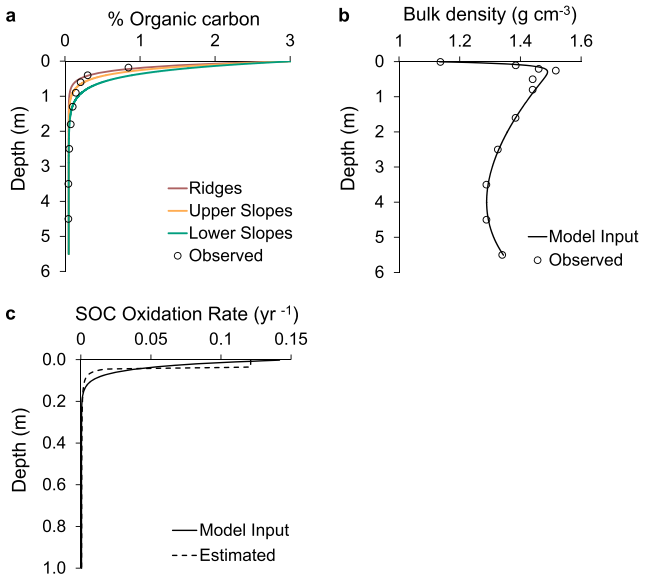

Figure 3. Exponential functions fitted to observations, to parsimoniously represent the depth variation of soil biogeochemical properties at multiple horizons: (a) organic carbon concentration, (b) bulk density, and (c) oxidation rate of organic carbon. The observations [*Billings et al*., 2010] were obtained from site G (Figure 2a). The variation of initial organic carbon concentration at different hillslope positions illustrated in Figure 3a corresponds to the topographic classification of Figure 2b. The initial depth-dependent SOC concentration at ridges was obtained by fitting equation (2) to the observations [*Billings et al*., 2010]. Assumptions on the depth dependence of initial organic carbon concentration at upper and lower slopes [*Rosenbloom et al*., 2006] are discussed in Appendix A. The associated parameters are given in the supplementary Table S1.

section 4.2). Mechanisms that induce advection-diffusion phenomena (e.g., bioturbation, tillage, and soil creep) may lead to the mixing of SOC content estimated by equation (1) across different horizons within the soil column [*Chaopricha and Marín-Spiotta*, 2014]. At each time step, the SOC depth variation is estimated by applying equation (B3), assuming mixing of the estimated SOC content (equation (1)) across soil horizons.

To quantify erosion-induced C fluxes, steady state conditions were assumed at the beginning of simulation, with zero net soil-atmosphere C exchange [*Billings et al*., 2010; *Jenny*, 1941; *Van Oost et al*., 2007]. This assumption represents the state of the ecosystem before the extensive forest cutover that started in the area in the late eighteenth century, which combined with inadequate soil management practices most likely led to the beginning of severe erosion of millions of hectares of land in the broader region [*Trimble*, 1974]. The model is initialized with estimates of depth-dependent soil bulk density, SOC oxidation rate, and SOC concentration. The SOC production term (equation (S1) in the supporting information) is assumed to exponentially decay with depth [*Yoo et al*., 2005; 2006] (see Text S2 in the supporting information for the estimation of the initial depth-dependent SOC production rate). Furthermore, in addition to the dependence of SOC on depth, the spatially explicit model considers the variation with topography. Deep C accumulation varies topographically depending on slope morphology. This work systematically accounts for topographic controls on the initial SOC content (Figure 2b) based on the analysis given by *Rosenbloom et al*. [2006] (see Appendix A).

4.2. Carbon Oxidation and Production Parameters: Sensitivity Analysis on Effects of Management Practices

The effect of land management practices on the interaction of erosion and soil-atmosphere C exchange is represented by the coefficients a_k and a_l for oxidation and production, respectively (see section 2.1). In order to clarify the role of a_k and a_l on the net C flux and to select a set of parameters to use in the watershed simulations, a preliminary sensitivity analysis was conducted on an eroding site, assuming a 1 mm yr^{-1} constant erosion rate in 100 year simulations. The total SOC difference (ΔSOC) for 100 years is illustrated in Figure 4, which reflects the net result of SOC production, oxidation, and loss to erosion, based on the proposed framework. Depending on the values of a_k and a_l different scenarios range from a net increase to a net loss of SOC at the eroding soil profile. High values of a_k (a_l) represent a rapid restoration of the altered k_t (l_t), while low values have little effect on eroded profiles. A high value of a_k combined with low a_l lead to a net C source (i.e., net flux of CO_2 from soil to atmosphere); low values of a_k combined with relatively high a_l may lead to a net C sink (Appendix B).

To assess the watershed's integrated response in terms of atmospheric CO_2 fluxes three scenarios were considered: (a) a maximum C sink scenario, (b) a maximum C source scenario, and (c) an intermediate scenario. For the maximum sink scenario, based on Figure 4 $a_l = 3\,g\,m^{-3}\,yr^{-1}$ (i.e., the value for a_l above which the SOC difference in Figure 4 does not significantly change) is used and a_k is minimized ($a_k = 0\,yr^{-1}$). Similarly,

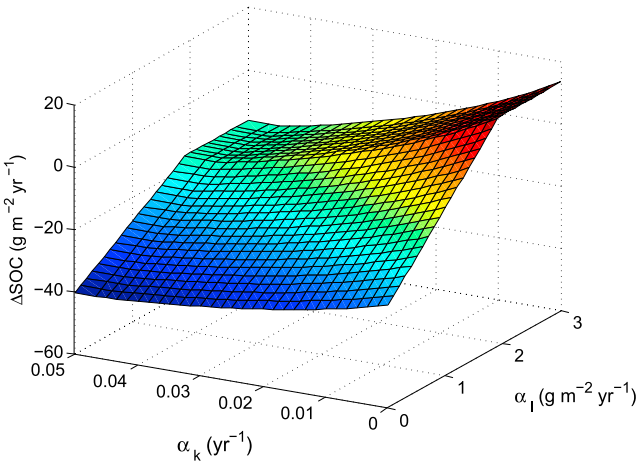

Figure 4. Sensitivity analysis on the effect of management practices to the total difference in soil organic carbon storage (ΔSOC). The net result of soil organic carbon (SOC) production, oxidation, and SOC loss to erosion is illustrated, as the effects of management practices on altered oxidation and production (a_k and a_l, respectively) vary. Positive values of ΔSOC indicate net increase of SOC at the eroding site, while negative values represent net SOC loss to the atmosphere and to erosion.

for the maximum source scenario $a_l = 0\,\mathrm{g\,m^{-3}\,yr^{-1}}$ and $a_k = 0.05\,\mathrm{yr^{-1}}$ are used. For the intermediate scenario we selected $a_l = 1.5\,\mathrm{g\,m^{-3}\,yr^{-1}}$ and $a_k = 0.025\,\mathrm{yr^{-1}}$. The simulated response surface of Figure 4 depends on the cumulative erosion for the time period of the simulation (100 years). This range of a_k and a_l values (see Table S1 in the supporting information) reflects plausible states of the ecosystem during its long agricultural history.

4.3. Land Surface Data

This work uses a digital elevation model (DEM) and information on the spatial distribution of vegetation from the *South Carolina Department of Natural Resources* [2009]. The fine (5 m) elevation data set appropriately depicts important topographic and hydrologic characteristics (e.g., contributing area, slope, and curvature) and is more recent than the one utilized by *James et al*. [2007] to map geomorphological characteristics of the area. A 30 m mesh of computational elements was obtained based on the 5 m DEM (Figure 2a). Note that the geomorphic model parameterization (section 4.6) accounts for the potential bias in the erosion capacity of the landscape resulting from initializing the simulation with a recent DEM. The soil classification map (Figure 2c) of the area was obtained from local soil surveys (http://websoilsurvey.nrcs.usda.gov/) conducted by the U.S. Department of Agriculture (USDA). Soil textural classes characterizing the area were grouped into three soil types according to the corresponding *U.S. Department of Agriculture* [1951] classification.

The vegetation map of the area is shown in Figure 2d. The watershed is covered by several kinds of forest stands: those dominated by loblolly pine (*Pinus taeda*) and shortleaf pine (*Pinus echinata*); mixed stands of hardwoods such as white oak (*Quercus alba*), northern red oak (*Quercus rubra*), and hickory (*Carya sp*.); and hardwoods such as sweetgum (*Liquidambar styraciflua*) and yellow poplar (*Liriodendron tulipifera*). The pine stands are modeled [*Hansen et al*., 2000] as evergreen needleleaf forest with a vegetation height of 30 m, while hardwood forests are modeled as deciduous broadleaf forest with a vegetation height of 25 m. In this first order modeling approach, the observed vegetation patterns are assumed time invariant. Selection of soil and ecological parameters is discussed in section 4.5 and in the supporting information.

4.4. Hydrometeorological Forcing and Validation of the Hydrologic Model

We conducted a 100 year simulation to study the hydro-geomorphic response of the watershed and the influence on soil-atmosphere C exchange. Observations of hydro-climatic variables were used as inputs to a weather generator [*Fatichi et al*., 2011] to produce a 100 year hydroclimatic scenario at the hourly scale (see the supporting information). Soil moisture data from site G (Figure 2a), obtained using gypsum blocks, were used to validate the hydrologic model's performance. Simulated soil moisture at site A (Figure 2a), which is characterized by similar surface properties as site G, is used for comparison. Description of the most essential soil hydraulic parameters in the hydrologic model and the initialization and validation procedures are discussed in the supporting information.

4.5. Biogeomorphic Properties

Geomorphic variables controlling raindrop impact detachment erosion, and overland flow erosion were selected from the literature [*Finney*, 1984; *Francipane et al*., 2012; *Meyer and Harmon*, 1984; *Yalin*, 1977]. The most important soil properties affecting soil erosion are the shear stress-based soil erodibility (K_b), the raindrop detachment soil erodibility (K_r), and the critical shear stress (τ_c). K_b expresses the soil tendency to

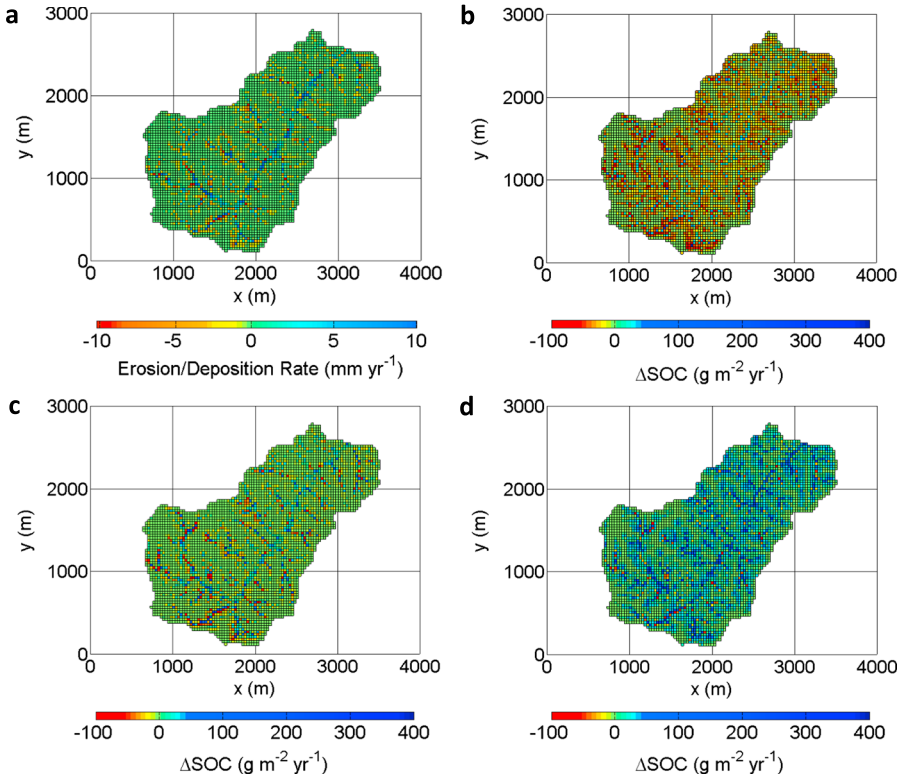

Figure 5. Spatially explicit representation of soil erosion and of soil organic carbon redistribution. (a) Higher sediment deposition rates are illustrated in blue (e.g., across the stream network), while eroding sites (yellow to red) dominate hillslopes. (b) Total difference in soil organic carbon storage (ΔSOC) across the landscape corresponding to the maximum source scenario (14.5 g C m^{-2} yr^{-1}), (c) the intermediate scenario (0.08 g C m^{-2} yr^{-1}), and (d) the maximum sink scenario (−18.2 g C m^{-2} yr^{-1}).

be eroded by overland flow. K_r characterizes how susceptible the soil is on rain splash erosion and depends on soil textural classes. τ_c is the threshold stress value associated with particle entrainment. Ecological parameters controlling rain splash erosion include the fraction of vegetation (v) of each computational element, the percentage of nonvegetated area (e.g., rock cover) protected against drop erosion (C_r), and the drip coefficient (F_l), which expresses the percentage of intercepted rainfall reaching the soil in the form of leaf drip. A detailed description on the structure of the geomorphic model is given by *Francipane* [2010] and by *Francipane et al.* [2012].

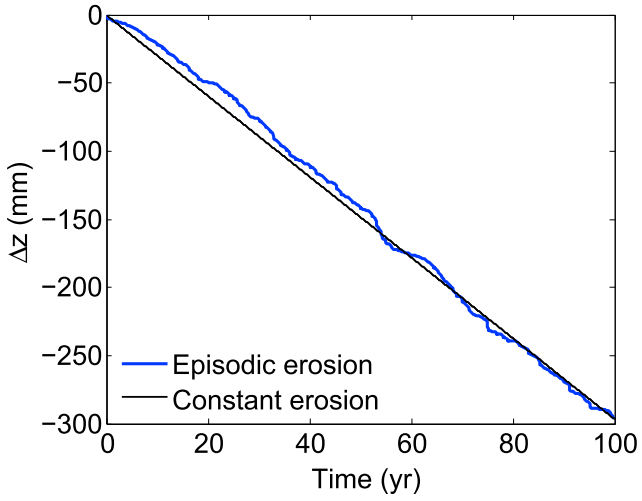

Figure 6. Temporal evolution of soil erosion at site A. The episodic character of soil erosion is evident (in blue), compared to the case of constant erosion (around 3 mm yr^{-1}, in black). Negative values of elevation change (Δz) denote erosion-induced net depression of soil surface, as a result from the 100 year hydro-meteorological forcing.

Starting from literature values, we tuned the soil and ecological parameters to mimic the history of severe erosion characterizing the area [*Trimble*, 1974], which led to the loss of the A horizon of many soil profiles [*Richter and Markewitz*, 2001]. This implies erosion rates of at least 1 mm yr^{-1} at eroding hillslopes across the Holcombe's Branch [*Billings et al.*, 2010]. The selected values of characteristic soil properties and ecological parameters are given in Tables S2 and S3, respectively.

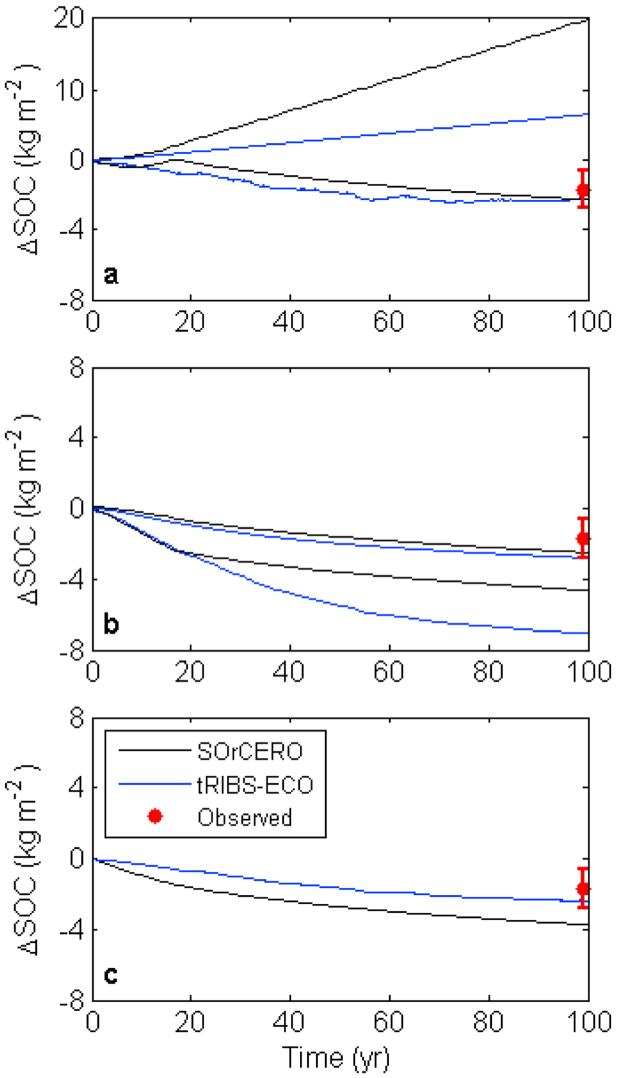

Figure 7. Temporal evolution of the difference in total profile soil organic carbon storage (ΔSOC) resulting from SOC fluxes at eroding site A for tRIBS-ECO (in blue) and for SOrCERO (in black), and ΔSOC based on the observations of Table 1 (red points; the associated range corresponds to 1 standard deviation). (a) Maximum sink and (b) maximum source scenarios for both models are illustrated. The positive vertical axis in Figure 7a is at a different scale. Positive and negative values of ΔSOC represent a net sink and source of atmospheric CO_2, respectively. In Figures 7a and 7b for each model we illustrate two extreme cases on the fate of eroded SOC: The series with relatively higher value of total ΔSOC correspond to the case where eroded SOC leaving the soil profile is completely oxidized during transport and burial; the series with relatively lower value of total ΔSOC correspond to the case where the eroded SOC is fully protected from oxidation (section 5.1). Depending on the fate of eroded SOC, estimates by the two scenarios are in the vicinity of the net C exchange with the atmosphere of the site. (c) Simulated net SOC losses to erosion corresponding to intermediate scenarios for the two models are compared against the observed ΔSOC. The quantitative equivalency of the illustrated intermediate scenarios is discussed in section 5.1. The episodic erosion in tRIBS-ECO leads to a closer representation of the history of SOC erosion of the site.

Results of a 100 year scenario of accelerated soil erosion and redistribution are illustrated in Figure 5a. Erosion rates in the vicinity of 1 mm yr^{-1} or higher dominate the watershed hillslopes (illustrated in yellow color in Figure 5a). Depositional sites are mainly located in the proximity to the stream network. The geomorphic model parameterization is directly linked to and depends on the calibration of the hydrologic model.

5. Results

5.1. Influence of Episodic Erosion on the Carbon Exchange With the Atmosphere

To assess the influence of episodic erosion on the redistribution of SOC we compared the results of tRIBS-ECO to those of SOrCERO, which uses an assumed constant erosion rate. Because SOrCERO operates at a point in the landscape, a heavily eroding site (site A in Figure 2a) was selected. We compared the C exchange with the atmosphere estimated by the two models for a 100 year scenario of severe erosion (section 4.4). Site A is characterized by a mean erosion rate of around 3 mm yr^{-1}. SOrCERO was initialized with depth-dependent SOC content, oxidation, and production rates corresponding to the undisturbed site discussed in section 4.1. A constant erosion rate of 3 mm yr^{-1} was assumed for SOrCERO. The erosion time series simulated by tRIBS-ECO at site A is illustrated in Figure 6. The episodic character of the hydro-meteorological forcing and the dynamic response of the watershed lead to time-varying soil erosion.

To represent different states of the ecosystem during its agricultural history, we studied a maximum C source and a maximum C sink scenario based on the effect of management practices on CO_2 release. In tRIBS-ECO the two scenarios are defined by the a_k and a_l values specified in section 4.2. In SOrCERO the corresponding scenarios are represented by the mixing coefficients n_{ox} and n_{prod} (described in section 2.3). Extreme values of the mixing coefficients (i.e., $n_{ox} = 0$ and $n_{prod} = 1$ for the maximum sink scenario, and $n_{ox} = 1$ and $n_{prod} = 0$ for the maximum source scenario) were selected, as discussed by *Billings et al.* [2010].

Table 1. Soil Organic Carbon (SOC) Content at Soil Profiles in Relatively Undisturbed Hardwood Stands and in Eroded Old-Field Pine Stands, at the Calhoun Critical Zone Observatory [*Billings et al*., 2010; *Markewitz and Richter*, 1998; *Richter and Markewitz*, 2001; *Richter et al*., 1999][a]

Depth (m)	SOC ($kg\,m^{-2}$)	SOC ($kg\,m^{-2}$)	ΔSOC ($kg\,m^{-2}$)
	Undisturbed Sites	Eroded Sites	
0–0.30	3.252 (0.24)	1.907 (0.13)	1.345 (0.62)
0.30–0.55	0.959 (0.18)	0.760 (0.32)	0.199 (1.49)
0.55–0.875	0.749 (0.33)	0.711 (0.54)	0.037 (12.2)
0.875–1.1	0.347 (0.47)	0.232 (0.28)	0.114 (1.54)
0–1.1	5.307 (0.18)	3.611 (0.16)	1.696 (0.65)

[a]Data from four soil profiles of each forest type were available. The coefficients of variation are given in parentheses. The estimated mean difference in SOC content (ΔSOC approximately equal to $1.7\,kg\,m^{-2}$) represents the cumulative SOC loss to erosion during the agricultural history of the area [*Trimble*, 1974].

The fate of eroded SOC is a crucial factor to quantifying the impact of erosion on the atmospheric CO_2 pool [*Harden et al*., 1999]. The influence of the decomposition of eroded SOC on soil-atmosphere C exchange has been studied by *Billings et al*. [2010], at a single eroding profile under different assumptions about management practices. However, SOrCERO does not explicitly track the dynamics of eroded SOC. Thus, assumptions are required about the fate of eroded SOC. These assumptions facilitate the point comparison between tRIBS-ECO and SOrCERO. Note that tRIBS-ECO operates at the watershed, not point, scale and does not require assumptions on the amount of eroded SOC that is protected from oxidation because its spatially (and thus topographically) explicit structure dictates that fate. Two extreme cases were considered for the two models: (1) all eroded SOC leaving the soil profile is completely oxidized during transport and burial [*Lal*, 1995] and (2) eroded SOC is stored in deeper horizons at depositional sites, inhibiting oxidation [*Smith et al*., 2001]. The two cases define the envelope of possible atmospheric CO_2 fluxes illustrated in Figure 7. tRIBS-ECO results corresponding to the two cases are also plotted in Figure 7. The illustrated series of C fluxes span the full range of scenarios regarding the fate of the eroded SOC. Thus, both for the maximum sink (Figure 7a) and maximum source (Figure 7b) scenarios (section 4.2), C fluxes obtained from the change in SOC between the uneroded profile (i.e., model start) and the model result after 100 years of erosion history for each model and assumption about the fate of eroded C illustrated in Figure 7. The tRIBS-ECO model thus yields a maximum source of $70.7\,g\,C\,m^{-2}\,yr^{-1}$ and a maximum sink of $-65.5\,g\,C\,m^{-2}\,yr^{-1}$, while the maximum source and sink values using SOrCERO were $46.3\,g\,C\,m^{-2}\,yr^{-1}$ and $-199.2\,g\,C\,m^{-2}\,yr^{-1}$, respectively. The range estimated by SOrCERO is markedly larger than the one estimated by tRIBS-ECO (section 6).

SOC content observations from four soil profiles in undisturbed hardwood stands were also compared with four profiles in eroded pine stands at the Calhoun Critical Zone Observatory [*Billings et al*., 2010; *Markewitz and Richter*, 1998; *Richter and Markewitz*, 2001; *Richter et al*., 1999] (Table 1). The soil profiles are not located within the Holcombe's Branch; observations of SOC content at depositional sites are not yet available. We estimate that the mean SOC loss to erosion is equal to $1.7\,kg\,m^{-2}$ (32% loss of the original SOC storage) and the coefficient of variation (defined as the ratio of the standard deviation over the mean) is equal to 0.65. This estimate represents the cumulative SOC loss to erosion during the agricultural history of the area [*Trimble*, 1974] and is equivalent to $17\,g\,C\,m^{-2}\,yr^{-1}$ over 100 years of agriculture. Figures 7a and 7b illustrate the observation-based ΔSOC (red points) and the associated spatial variation (1 standard deviation), in comparison to the maximum sink and maximum source scenarios, respectively. For the maximum sink scenario, simulations corresponding to different assumptions about the fate of eroded SOC encompass the ΔSOC inferred from observations. For the maximum source scenario, the simulations that assume protection of eroded SOC from oxidation ($2.8\,kg\,m^{-2}$ C loss for tRIBS-ECO and $2.5\,kg\,m^{-2}$ for SOrCERO, respectively) are not statistically different from observations.

The performance of the two models at site A for an intermediate scenario of SOC fluxes was contrasted. For tRIBS-ECO the intermediate scenario discussed in section 4.2 was used. For SOrCERO n_{ox} and n_{prod} values equal to 0.5 [*Billings et al*., 2010] were used. The quantitative equivalency of the two model runs is clear by comparing the result of Figure 4 (for $a_l = 1.5\,g\,m^{-3}\,yr^{-1}$ and $a_k = 0.025\,yr^{-1}$) with the sensitivity analysis of n_{ox} and n_{prod} conducted by *Billings et al*. [2010]. The simulated time series of SOC loss to erosion is shown in Figure 7c. While SOrCERO significantly overestimated the net erosion-induced SOC loss ($3.7\,kg\,m^{-2}$), the mean SOC flux predicted by tRIBS-ECO ($2.4\,kg\,m^{-2}$) is within 1 standard deviation of the observation-based ΔSOC ($1.7\,kg\,m^{-2}$). In this point comparison the two models were initialized in the same manner (i.e., with data from the undisturbed site discussed in section 4.1), and the time average of the erosion rate is the same (around $3\,mm\,yr^{-1}$)

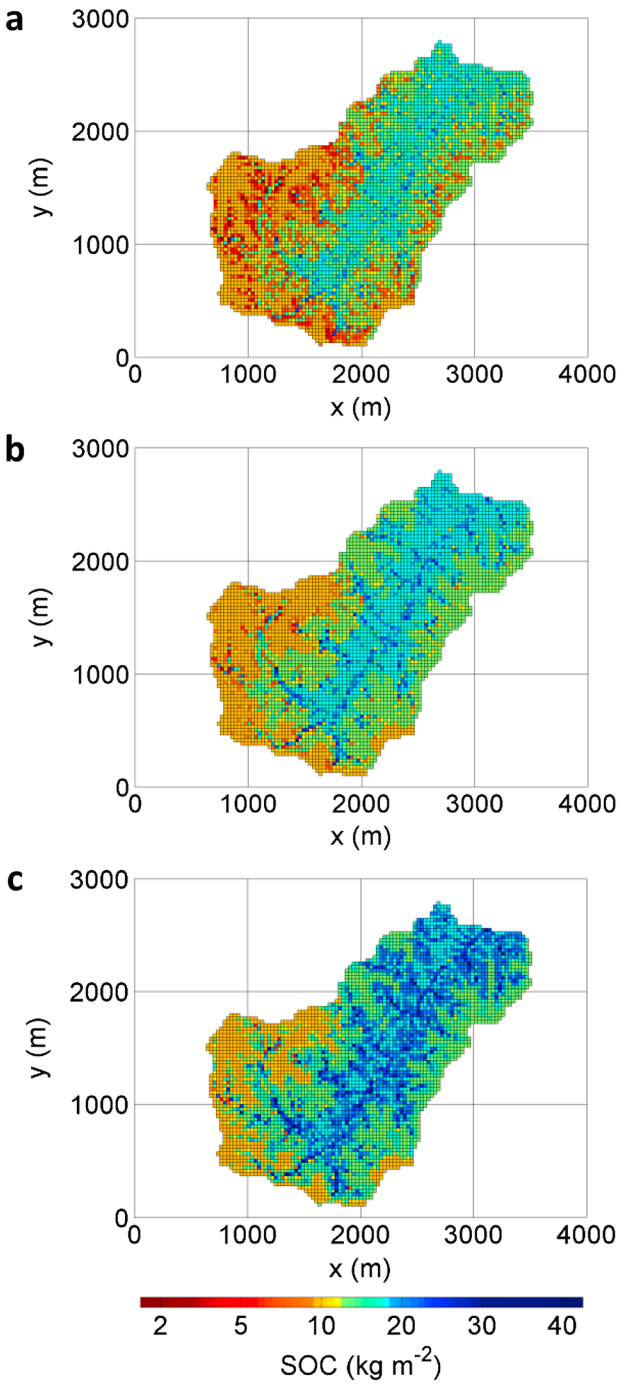

Figure 8. Topographic variation of simulated soil organic carbon storage across the watershed. Total soil organic carbon (SOC) storage at the upper 5 m of soil is illustrated for the (a) maximum source, (b) intermediate, and (c) maximum sink scenarios, respectively (section 5.2).

in the two simulations. The most important structural difference between the two models is the assumed constant erosion in SOrCERO versus the time-varying erosion in tRIBS-ECO. The more satisfactory performance of tRIBS-ECO is attributed to its ability to depict episodic SOC erosion at fine time scales. The episodic erosion significantly affects the lateral C flux and the dynamics of oxidation and production of SOC, compared to the assumption of constant erosion [*Billings et al.*, 2010].

5.2. Watershed-Integrated Analysis

The watershed-integrated hydro-geomorphic response of Holcombe's Branch and the erosion-induced soil-atmosphere CO_2 flux were modeled using tRIBS-ECO. The model was forced with the 100 year hydroclimatic scenario discussed in section 4.4 (see also the supporting information). The effect of management practices on the interaction of erosion and soil-atmosphere C flux was illustrated using the maximum source, intermediate, and maximum sink scenarios discussed in section 4.2. Spatially explicit results for the three scenarios are presented in Figure 5, illustrating the difference between the initial and final SOC storage at each computational element. The total SOC storage predicted in 5 m of soil for the three scenarios is illustrated in Figure 8. Watershed-integrated results yielded a 14.5 g C m^{-2} yr^{-1} source for the maximum source scenario, a −18.2 g C m^{-2} yr^{-1} sink for the maximum sink scenario, and a relatively small (0.08 g C m^{-2} yr^{-1} source) net C exchange with the atmosphere for the intermediate scenario. Results correspond to 100 year mean C fluxes averaged over the watershed area. The simulated range of erosion-induced soil-atmosphere C exchange estimates is in agreement with other published estimates (Table 2). Significant SOC loss is evident across hillslopes for the maximum source scenario (Figures 5b and 8a). For the intermediate scenario (Figures 5c and 8b) there are losses of SOC at eroding hillslopes and increases in the amount of SOC at depositional sites, across the stream network (statistics of ΔSOC are given in Table 3). For the maximum sink scenario relatively higher SOC content at the surficial horizons of eroding sites leads to larger amounts of SOC in the mobilized sediment (Figures 5d and 8c). The SOC loss to erosion estimated from observations (17 g m^{-2} yr^{-1}) is in the vicinity of the simulated range of C fluxes, even though the exact fraction of the eroded SOC that contributed to atmospheric CO_2 cannot be determined.

Table 2. Comparison of Watershed-Integrated Estimates of the Net Soil-Atmosphere C Exchange With Published Estimates[a]

Source	Range
tRIBS-ECO	−18.2 to 14.5
Harden et al. [1999]	−10 to −20
Yoo et al. [2005]	−1.7 to −2.8
Van Oost et al. [2005]	−3 to −10
Jacinthe and Lal [2001]	6 to 52

[a]Positive and negative values correspond to net erosion-induced C sources and sinks, respectively (values in g C m^{-2} yr^{-1}).

We also estimated the proportion of eroding C replaced by newly sequestered C [*Harden et al.*, 1999; *Stallard*, 1998] across the watershed. We analyzed the ratio of net vertical (i.e., exchange between the soil profile and the atmosphere) to lateral C fluxes at eroding sites across the watershed for the 100 year intermediate scenario (Figure 9), which is more representative of the C exchange with the atmosphere at eroding sites (demonstrated in section 5.1). Table 3 gives the statistical properties of the total eroded and replaced SOC at eroding sites, respectively. On average, 34% of eroded C has been replaced by C sequestration. The results highlight the wide topographic variability of C replacement across sites with varying hillslope morphology (Figure 9).

6. Discussion

6.1. Erosion-Induced Soil-Atmosphere Carbon Exchange

This work models movement of SOC across the landscape as induced by accelerated erosion and how erosion and lateral SOC redistribution (Figures 5 and 8) exhibit significant spatial heterogeneity controlled by hillslope characteristics, variation of soil physical and biochemical properties, and management practices. Severe erosion can transfer subsoil from eroding to depositional sites, and the reallocated sediment can bury formerly surficial horizons at depositional areas [*Quinton et al.*, 2010; *Stallard*, 1998; *Van Oost et al.*, 2005]. This process combined with advection/diffusion phenomena among different horizons results in continuously evolving vertical profiles of SOC. Consequently, in agreement with *Van Oost et al.* [2007], sampling of deeper C storage is required to strengthen previous conclusions that rely on measurements at surficial horizons.

Based on the significant topographic variability of C fluxes presented in our results (section 5.2), we highlight the strong control that slope morphology exerts on the redistribution of SOC as a function of erosion and deposition. Systematically tracking the dynamics of eroded SOC across the landscape (section 5.1) is critical for estimating the strength of erosion-induced atmospheric CO_2 flux [*Harden et al.*, 1999; *Van Oost et al.*, 2007]. In the proposed framework, eroded SOC is redistributed across the landscape and can experience oxidation upon transport or storage at depositional sites. Our analysis demonstrates that SOC burial at depositional sites is either short-term [*Van Oost et al.*, 2012] or long-term, depending on geomorphological characteristics, the rate of sediment transport, and oxidation rates at depositional sites. This representation of spatial heterogeneity of erosion and of the dynamics of mobilized SOC is an important improvement to studies based on conceptual scenarios regarding the fate of eroded SOC [*Billings et al.*, 2010; *Lal*, 1995; *Smith et al.*, 2001].

To quantify the influence of the proposed spatially explicit, physically based representation of C erosion and deposition on the net atmospheric CO_2 flux, a comparison with the SOrCERO model (section 5.1) was carried out at the watershed scale for the 100 year scenario of severe erosion discussed in section 4.4. The SOrCERO annual erosion rate was fixed at 1 mm yr^{-1} characterizing eroding sites at the Holcombe's Branch [*Billings et al.*, 2010], and the input data given in Figure 3 were used. Maximum sink and maximum source scenarios were considered for SOrCERO, which provided a maximum net C source and sink of 27.5 g m^{-2} yr^{-1} and −53.7 g m^{-2} yr^{-1}, respectively. This range encompasses the SOC loss of 17 g C m^{-2} yr^{-1} deduced from observations (section 5.1), yet is markedly larger than the range estimated by tRIBS-ECO (i.e., maximum net C source and sink strength of

Table 3. Statistics of the Total Eroded and Replaced Soil Organic Carbon (SOC) at Eroding Sites, and of the Net Total SOC Difference (ΔSOC) at the Watershed Scale for the 100 Year Intermediate Scenario (Values in kg m^{-2})

	Eroding Sites		Watershed Scale
	Eroded SOC	Replaced SOC	ΔSOC
Mean	0.97	0.38	0.01
Standard deviation	1.52	0.56	1.59
Minimum	0	0	-8.14
Maximum	8.66	2.18	17.26

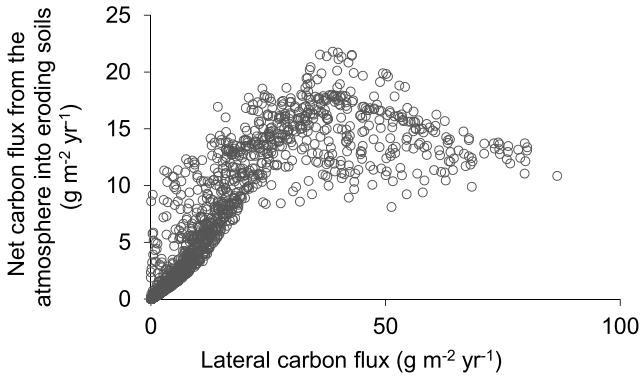

Figure 9. Net carbon flux into eroding soils due to replacement by vegetation inputs versus erosion-induced lateral carbon flux. This figure illustrates the wide topographic variation of carbon (C) fluxes across the landscape for the intermediate scenario. Thirty-four percent of the eroding C is being replaced by sequestered C from the atmosphere. A significant coefficient of variation (defined as the ratio of standard deviation over the mean) of around 8 characterizes the large natural spatial variability of the C replacement ratio (i.e., the ratio of C uptake over C loss to erosion).

14.5 and $-18.2\,g\,m^{-2}\,yr^{-1}$, respectively). The approach implemented in tRIBS-ECO is more faithful to the actual erosion-inducing mechanisms and involves a significantly more detailed description of the study area (see section 4). We attribute the large discrepancies to the inability of SOrCERO to constrain the range of possible C fluxes by accounting for the fate of eroded SOC, including the role of depositional sites in storing eroded SOC, and by representing time-varying erosion (section 5.1).

6.2. Episodic Erosion of Soil Organic Carbon

The watershed's response to hydrometeorological events leads to episodic events on soil erosion. The magnitude and frequency of erosion events control lateral C losses [*Dlugoß et al.*, 2012]. This study accounts for the episodic character of erosion rates resulting from the watershed's hydro-geomorphic response to hydro-meteorological forcings at the hourly time scale. We demonstrate the potential of a time-varying representation of erosion and management practices on assessing the SOC redistribution across a watershed and quantifying the net atmospheric CO_2 flux. For this purpose, we used a point comparison at an eroding profile of the results of tRIBS-ECO and SOrCERO, the latter assuming a constant erosion rate. The simulated scenarios were evaluated based on SOC erosion inferred from observations at the site (section 5.1). In this point comparison, different assumptions about management practices and the fate of eroded SOC (Figure 7) lead to a relatively wide range of erosion-induced C fluxes. Accounting for effects of episodic erosion in estimates of net soil-atmosphere C exchange may lead to a significantly more constrained range of possible C fluxes compared to the case when a constant erosion rate is assumed. More precisely, while the maximum source strength estimated by SOrCERO is 35% lower than the one obtained by the proposed approach, the maximum sink strength is more than 3 times greater than the one estimated by tRIBS-ECO. As a result, the total range of possible C fluxes estimated by SOrCERO is 80% larger than the one estimated by tRIBS-ECO (Figure 7). Depending on the fate of eroded SOC, the extreme scenarios may approximate the net C exchange with the atmosphere that characterized the site during its agricultural history [*Trimble*, 1974]. The extent to which eroded SOC is oxidized upon transport and burial has an important role in the erosion-induced C sink or source strength [*Billings et al.*, 2010]. There is a clear need to systematically track the dynamics of eroded SOC to accurately estimate the net soil-atmosphere C exchange. Moreover, it is reasonable that changes in management practices and land uses [*Trimble*, 1974] may lead to a transition between an erosion-induced net C source and a net C sink over time [*Harden et al.*, 1999; *Van Oost et al.*, 2012].

Accounting for time-varying erosion may lead to a more accurate representation of the total SOC losses to erosion at the site. We evaluated the performance of the two models to mimic the SOC erosional history of site A for an intermediate scenario of C fluxes (section 5.1). While SOrCERO overestimated the SOC loss to erosion by more than twice, the C loss estimate of tRIBS-ECO is significantly closer to the observed one. This point comparison demonstrates that the episodic representation of erosion and management practices can have a meaningful impact on soil-atmosphere CO_2 exchange and hence should be taken into account in studies assessing the influence of erosion on the C cycle. Neglecting the fine temporal dynamics associated with the episodic character of natural erosion-inducing mechanisms [*Billings et al.*, 2010; *Liu et al.*, 2003; *Rosenbloom et al.*, 2006; *Van Oost et al.*, 2005; *Yoo et al.*, 2005] may significantly affect estimates of the net C exchange with the atmosphere.

6.3. Spatial Variation of Carbon Replacement

Assumptions about the proportion of eroding C replaced by newly sequestered C ("dynamic replacement" [*Harden et al.*, 1999; *Stallard*, 1998]) vary in the literature [*Harden et al.*, 1999; *Smith et al.*, 2001; *Van Oost*

et al., 2007] leading to markedly different conclusions on the net C exchange with the atmosphere. Results for the intermediate indicate that 34% of the eroding C across the watershed has been replaced by sequestered C from the atmosphere, which is consistent with the range of 11% to 55% reported in the global study of *Van Oost et al*. [2007]. The associated replacement mainly occurs at the active SOC pool with turnover times up to decades [*Harden et al*., 1999; *Van Oost et al*., 2007]. Although accounting for preferential erosion of varying sized soil aggregates is out of the scope of this study, preferential erosion of soil particles (e.g., nutrient-rich clays with relatively high moisture retention capacity) can lead to changes in soil characteristics at the eroding site, altering the ability to produce and store SOC [*Billings et al*., 2010; *Hu and Kuhn*, 2014]. Erosion of surficial horizons may reduce the potential of the remaining soil system to promote SOC production [*Billings et al*., 2010]. As a result, in unfertilized systems C inputs at eroding sites may decline relative to their preerosion rate [*Harden et al*., 1999]. In contrast, in managed systems fertilization may enhance system productivity at eroding sites [*Harden et al*., 1999; *Stallard*, 1998]. The moderating effect of management practices on altered SOC production at eroding sites [*Billings et al*., 2010] is explicitly accounted for by the proposed framework in the simulated scenarios.

This study stresses the role of small-scale dynamics of soil erosion driven by topography on the variability of C fluxes. SOC replacement varies across the landscape depending on a multitude of factors including SOC content, oxidation rate, and bulk density, and it can be influenced by management practices, as episodic erosion proceeds. The distinctive (hook-shaped) pattern formed by the relationship between net lateral C loss at eroding sites and net C influx from the atmosphere to the soil (Figure 9) suggests high erosion rates such as those occurring on steep hillslopes can promote C losses to a greater extent than SOC can be regenerated. These sites correspond to points in Figure 5c with relative higher net lateral C loss. The wide topographic variation (Table 3) depicts the strong control hillslope morphology exerts on the soil's ability to store sequestered atmospheric C. This highlights the significant spatial variability of the associated C fluxes, which cannot be reflected in studies focusing at a single eroding site [*Billings et al*., 2010].

The natural variability on the C replacement ratio across the watershed can be quantified by a coefficient of variation of approximately equal to 8. The strong variation of C replacement (Figure 9) at small spatial scales (tens of meters) is comparable to that reported by *Van Oost et al*. [2007], who conducted an analysis of 1400 profile measurements. The results of this study were obtained for various settings of hillslope characteristics, based on a detailed representation of episodic and spatially heterogeneous soil erosion. We attribute the large spatial variability of soil-atmosphere C flux to the complexity of erosion-inducing processes at small scales, which exerts a strong control on depth-dependent biogeochemical properties of soils, including SOC oxidation and production.

6.4. Future Research

The erosion-induced soil-atmosphere C exchange can be better quantified with additional SOC measurements within Holcombe's Branch. Given the significant topographic variability of C fluxes demonstrated in this study, future sampling campaigns will focus on various positions across the catena [*Rosenbloom et al*., 2006]. Measurements from interfluves, slopes, and depositional sites will help in evaluating the capacity of tRIBS-ECO to efficiently reproduce C inventories and decomposition rates at the study site. The coupled and physically based character of tRIBS-ECO allows the quantification of dynamic feedback among hydro-geomorphic and biogeochemical processes at fine temporal and spatial scales to test multiple hypotheses. tRIBS-ECO can be used to evaluate seasonal or long-term controls of ecological, hydrological, and biogeochemical processes [*Richter and Billings*, 2015]. The uncertainty associated with the natural spatial variability of hydrological, geomorphological, and biogeochemical properties can be significant [*Arnone et al*., 2014; 2016] and needs to be accounted for in estimates of atmospheric C fluxes derived from erosional processes. tRIBS-ECO can also be used to assess how topography among contrasting depositional environments may influence the degree to which eroded SOC may be preserved. Given our lack of knowledge about the fate of most eroded SOC on time scales of decades to centuries, this is of particular interest for future studies. Investigations addressing these issues are especially compelling in areas where erosion has been accelerated by anthropogenic activity, and in sites where extreme hydro-meteorological phenomena and geomorphic gradients have the potential to induce significant sediment transport [*Dialynas et al*., 2015].

7. Conclusions

1. A parsimonious, spatially and depth-explicit biogeochemical model (tRIBS-ECO) is introduced. It is used to examine whether soil erosion at the landscape scale enhances net C sequestration or CO_2 return to the atmosphere. The physically based representation of the spatial heterogeneity of erosion and of the dynamics of mobilized SOC has a significant influence on the net soil-atmosphere C exchange.
2. Observations suggest that 32% of the original SOC content at the study area has been eroded. The episodic representation of erosion reproduced the SOC loss in eroded sites better than a model that assumed a constant erosion rate, suggesting that time-varying erosion may be an important feature for accurate representation of erosion-induced SOC dynamics.
3. Models indicate that land use practices (e.g., fertilization and associated enhancement of system productivity) can have a substantial influence on SOC production and oxidation rates at eroding sites, which can significantly impact the net C exchange with the atmosphere.
4. Watershed-integrated estimates of erosion-induced net atmospheric C fluxes ranged from a source strength of $14.5\,\mathrm{g\,C\,m^{-2}\,yr^{-1}}$ to a sink strength of $-18.2\,\mathrm{g\,C\,m^{-2}\,yr^{-1}}$, encompassing the observation-based SOC flux. On average, 34% of eroded C has been replaced by C sequestration at the intermediate scenario.
5. The simulated topographic variation of the C replacement at small spatial scales is comparable to the variability among multiple point estimates reported in a global-scale study. The strong spatial heterogeneity is attributed to the small-scale complexity of natural processes that drive C erosion. This variability is sometimes partially neglected with landscape- or global-scale studies that are often based on domain averaged C fluxes, or on scarce point measurements, yet it appears to be an important feature to consider in modeling efforts.
6. Although such an approach necessarily adds significant complexity to modeling efforts, accounting for small-scale heterogeneity in topography and temporally varying erosion rates can impart meaningful influence on model projections of erosion-induced, vertical, and lateral SOC fluxes and resulting SOC profile storage. We suggest that future attempts to quantify net C exchange with the atmosphere in regional and global C budgets incorporate hydrological, geomorphological, and biogeochemical drivers of C dynamics as erosion proceeds.

Appendix A: Additional Material on the Topographic Variation of Initial C Content

Rosenbloom et al. [2006] fitted exponential depth profiles of C concentration (similar to equation (2)) to observations across different landscape positions. They reported that C concentration attenuates rapidly with depth in ridges in comparison to middle slopes, while lower slopes exhibit slower depth attenuation. They represent the C attenuation at each location with different coefficients of exponential decay with depth (equivalent to C_b in equation (2)).

In this work the depth-dependent C content at the Holcombe's Branch's ridges is initialized based on observations [*Billings et al.*, 2010] illustrated in Figure 3a. The depth attenuation of initial C concentration at upper and lower slopes is captured by using different values for C_b (exponential decay of C concentration with depth). More specifically, the ratio of C_b corresponding to upper slopes over the C_b that corresponds to ridges was assumed equal to the one *Rosenbloom et al.* [2006] derived from observations. This method was also applied for the estimation of the depth attenuation of initial C concentration at lower slopes. The initial spatial distribution of C content and the depth-dependence of C concentration at different topographic locations are illustrated in Figures 2b and 3a, respectively. The associated parameters are given in Table S1.

Appendix B: Additional Material on the Estimation of SOC Content at Each Time Step

In the proposed approach, the depth-dependent SOC content is estimated at each time step by calculating the parameter $C_{a,t}$ in equation (2) based on the SOC difference given by equation (1). More precisely, the total SOC content (per unit area) is given by (see section 2.1 for notation):

$$\mathrm{SOC}_t = \int_0^{H_t} C_t(z)\rho(z)dz \tag{B1}$$

Substituting $C_t(z)$ from equation (2) yields

$$\mathrm{SOC}_t = \int_0^{H_t} \left(C_{a,t} e^{C_b z} + C_c\right)\rho(z)dz = C_{a,t}\left(\frac{\rho(z)\left(e^{C_b H_t} - 1\right)}{C_b}\right) + C_c H_t \rho(z) \quad \text{(B2)}$$

At time step $t+1$, the SOC content is estimated by applying equation (1). The value of $C_{a,t+1}$ is then calculated from equation (B2) as following:

$$C_{a,t+1} = \frac{C_b(SOC_{t+1} - C_c H_{t+1}\rho(z))}{\rho(z)(e^{C_b H_{t+1}} - 1)} \quad \text{(B3)}$$

Expressing $C_{a,t}$ as a time variant parameter implies mixing among surficial horizons in the soil column (see section 4.1). Equation (B3) is applied at eroding and depositional sites across the watershed.

Acknowledgments

Data supporting Figure 2 are available from the U.S. Department of Agriculture (http://websoilsurvey.nrcs.usda.gov/) and from the South Carolina Dep. of Natural Resources (http://coast.noaa.gov/dataviewer). The soil moisture measurements supporting Figure S1 are available at http://criticalzone.org/calhoun/data/. Data supporting Figure 3 were obtained as discussed in section 8. The hydrometeorological data used are available from the National Oceanic and Atmospheric Administration (National Center of Environmental Information, http://www.ncdc.noaa.gov/cdo-web/datasets). This work was supported by the National Science Foundation under the Calhoun Critical Zone Observatory effort (project EAR1331846). R.L. Bras acknowledges the support of the K. Harrison Brown Family Chair. The authors would like to thank S. Trumbore, C. Lehmeier, and two anonymous reviewers for their substantial and constructive comments.

References

Arnone, E., Y. G. Dialynas, L. V. Noto, and R. L. Bras (2014), Parameter uncertainty in shallow rainfall-triggered landslide modeling at basin scale: A probabilistic approach, *Proc. Earth Planet. Sci.*, *9*, 101–111, doi:10.1016/j.proeps.2014.06.003.

Arnone, E., Y. G. Dialynas, L. V. Noto, and R. L. Bras (2016), Accounting for soils parameter uncertainty in a physically based and distributed approach for rainfall-triggered landslides, *Hydrol. Process.*, *30*(6), 927–944, doi:10.1002/hyp.10609.

Battin, T. J., S. Luyssaert, L. A. Kaplan, A. K. Aufdenkampe, A. Richter, and L. J. Tranvik (2009), The boundless carbon cycle, *Nat. Geosci.*, *2*(9), 598–600, doi:10.1038/ngeo618.

Billings, S. A., R. W. Buddemeier, D. D. Richter, K. Van Oost, and G. Bohling (2010), A simple method for estimating the influence of eroding soil profiles on atmospheric CO2, *Global Biogeochem. Cycles*, *24*, GB2001, doi:10.1029/2009GB003560.

Chaopricha, N. T., and E. Marín-Spiotta (2014), Soil burial contributes to deep soil organic carbon storage, *Soil Biol. Biochem.*, *69*, 251–264, doi:10.1016/j.soilbio.2013.11.011.

Coleman, K., D. S. Jenkinson, G. J. Crocker, P. R. Grace, J. Klír, M. Körschens, P. R. Poulton, and D. D. Richter (1997), Simulating trends in soil organic carbon in long-term experiments using RothC-26.3, *Geoderma*, *81*(1), 29–44, doi:10.1016/S0016-7061(97)00079-7.

Dialynas, Y. G., S. Bastola, S. A. Billings, and R. L. Bras (2014), Assessing the impact of landscape evolution on carbon dynamics: A coupled physically based modelling approach, Abstract H42C-03 presented at 2014 Fall Meeting, AGU, San Francisco, Calif., 15–19 Dec.

Dialynas, Y. G., S. Bastola, R. L. Bras, E. Marín-Spiotta, W. L. Silver, E. Arnone, and L. V. Noto (2015), Influence of soil erosion and landslide occurrence on soil organic carbon storage and loss in the Luquillo Critical Zone Observatory, Puerto Rico, Abstract EP23C-0987 presented at 2015 Fall Meeting, AGU, San Francisco, Calif., 14–18 Dec.

Dlugoß, V., P. Fiener, K. Van Oost, and K. Schneider (2012), Model based analysis of lateral and vertical soil carbon fluxes induced by soil redistribution processes in a small agricultural catchment, *Earth Surf. Processes Landforms*, *37*(2), 193–208, doi:10.1002/esp.2246.

Doetterl, S., K. Van Oost, and J. Six (2012), Towards constraining the magnitude of global agricultural sediment and soil organic carbon fluxes, *Earth Surf. Processes Landforms*, *37*(6), 642–655, doi:10.1002/esp.3198.

Fatichi, S., V. Y. Ivanov, and E. Caporali (2011), Simulation of future climate scenarios with a weather generator, *Adv. Water Resour.*, *34*(4), 448–467, doi:10.1016/j.advwatres.2010.12.013.

Finney, H. J. (1984), The effect of crop covers on rainfall characteristics and splash detachment, *J. Agric. Eng. Res.*, *29*(4), 337–343, doi:10.1016/0021-8634(84)90089-1.

Francipane, A. (2010), tRIBS-Erosion: a physically-based model for studying mechanisms of eco-hydro-geomorphic coupling, PhD thesis, Univ. of Palermo, Italy.

Francipane, A., V. Y. Ivanov, L. V. Noto, E. Istanbulluoglu, E. Arnone, and R. L. Bras (2012), tRIBS-Erosion: A parsimonious physically-based model for studying catchment hydro-geomorphic response, *Catena*, *92*, 216–231, doi:10.1016/j.catena.2011.10.005.

Garrote, L., and R. L. Bras (1995), A distributed model for real-time flood forecasting using digital elevation models, *J. Hydrol.*, *167*, 279–306, doi:10.1016/0022-1694(94)02592-Y.

Hansen, M. C., R. S. Defries, J. R. G. Townshend, and R. Sohlberg (2000), Global land cover classification at 1 km spatial resolution using a classification tree approach, *Int. J. Remote Sens.*, *21*(6–7), 1331–1364, doi:10.1080/014311600210209.

Harden, J. W., J. M. Sharpe, W. J. Parton, D. S. Ojima, T. L. Fries, T. G. Huntington, and S. M. Dabney (1999), Dynamic replacement and loss of soil carbon on eroding cropland, *Global Biogeochem. Cycles*, *13*(4), 885–901, doi:10.1029/1999GB900061.

Hu, Y., and N. J. Kuhn (2014), Aggregates reduce transport distance of soil organic carbon: Are our balances correct?, *Biogeosciences*, *11*(22), 6209–6219, doi:10.5194/bgd-11-8829-2014.

Ivanov, V. Y., E. R. Vivoni, R. L. Bras, and D. Entekhabi (2004a), Preserving, high-resolution surface and rainfall data in operational-scale basin hydrology: A fully-distributed physically based approach, *J. Hydrol.*, *298*, 80–111, doi:10.1016/j.jhydrol.2004.03.041.

Ivanov, V. Y., E. R. Vivoni, R. L. Bras, and D. Entekhabi (2004b), Catchment hydrologic response with a fully distributed triangulated irregular network model, *Water Resour. Res.*, *40*, W11102, doi:10.1029/2004WR003218.

Jacinthe, P. A., and R. Lal (2001), A mass balance approach to assess carbon dioxide evolution during erosional events, *Land Degradation Dev.*, *12*(4), 329–339, doi:10.1002/ldr.454.

James, L. A., D. G. Watson, and W. F. Hansen (2007), Using LiDAR data to map gullies and headwater streams under forest canopy: South Carolina, USA, *Catena*, *71*(1), 132–144, doi:10.1016/j.catena.2006.10.010.

Jenny, H. (1941), *Factors of Soil Formation: A System of Quantitative Pedology*, pp. 269, McGraw-Hill, New York.

Lal, R. (1995), Global soil erosion by water and carbon dynamics, in *Soils and Global Change*, edited by R. Lal et al., pp. 131–141, CRC/Lewis Boca Raton, FL.

Lal, R. (2003), Soil erosion and the global carbon budget, *Environ. Int.*, *29*(4), 437–450, doi:10.1016/S0160-4120(02)00192-7.

Lal, R. (2004), Soil carbon sequestration to mitigate climate change, *Geoderma*, *123*(1–2), 1–22, doi:10.1016/j.geoderma.2004.01.032.

Liu, S., N. Bliss, E. Sundquist, and T. G. Huntington (2003), Modeling carbon dynamics in vegetation and soil under the impact of soil erosion and deposition, *Global Biogeochem. Cycles*, *17*(2), 1074, doi:10.1029/2002GB002010.

Markewitz, D., and D. D. Richter (1998), The bio in aluminum and silicon geochemistry, *Biogeochemistry*, *42*(1–2), 235–252, doi:10.1023/A:1005901417165.
Meyer, L. D., and W. C. Harmon (1984), Susceptibility of agricultural soils to interrill erosion, *Soil Sci. Soc. Am. J.*, *48*(5), 1152–1157, doi:10.2136/sssaj1984.03615995004800050040x.
Ni, J., Y. Yue, A. G. L. Borthwick, T. Li, C. Miao, and X. He (2012), Erosion-induced CO2 flux of small watersheds, *Global Planet. Change*, *94–95*, 101–110, doi:10.1016/j.gloplacha.2012.07.003.
Quinton, J. N., G. Govers, K. Van Oost, and R. D. Bardgett (2010), The impact of agricultural soil erosion on biogeochemical cycling, *Nat. Geosci.*, *3*(5), 311–314, doi:10.1038/ngeo838.
Regnier, P., et al. (2013), Anthropogenic perturbation of the carbon fluxes from land to ocean, *Nat. Geosci.*, *6*(8), 597–607, doi:10.1038/ngeo1830.
Richter, D. D., and S. A. Billings (2015), 'One physical system': Tansley's ecosystem as Earth's critical zone, *New Phytol.*, *206*(3), 900–912, doi:10.1111/nph.13338.
Richter, D. D., and D. Markewitz (2001), *Understanding Soil Change*, pp. 255, Cambridge Univ. Press, Cambridge, U. K.
Richter, D. D., D. Markewitz, S. E. Trumbore, and C. G. Wells (1999), Rapid accumulation and turnover of soil carbon in a re-establishing forest, *Nature*, *400*(6739), 56–58, doi:10.1038/21867.
Richter, D. D., H. L. Allen, J. Li, D. Markewitz, and J. Raikes (2006), Bioavailability of slowly cycling soil phosphorus: Major restructuring of soil P fractions over four decades in an aggrading forest, *Oecologia*, *150*(2), 259–271, doi:10.1007/s00442-006-0510-4.
Richter, D. D., et al. (2014), Evolution of soil, ecosystem, and critical zone research at the USDA FS Calhoun Experimental Forest, in *USDA Forest Service Experimental Forests and Ranges*, edited by D. C. Hayes et al., pp. 405–433, Springer, New York.
Rosenbloom, N. A., J. W. Harden, J. C. Neff, and D. S. Schimel (2006), Geomorphic control of landscape carbon accumulation, *J. Geophys. Res.*, *111*, G01004, doi:10.1029/2005JG000077.
SCDNR (2009), South Carolina Dep. of Natural Resources, 2008 South Carolina Lidar: Union County, National Oceanic and Atmospheric Administration. [Available at http://coast.noaa.gov/dataviewer.]
Smith, S. V., W. H. Renwick, R. W. Buddemeier, and C. J. Crossland (2001), Budgets of soil erosion and deposition for sediments and sedimentary organic carbon across the conterminous United States, *Global Biogeochem. Cycles*, *15*(3), 697–707, doi:10.1029/2000GB001341.
Stallard, R. F. (1998), Terrestrial sedimentation and the carbon cycle: Coupling weathering and erosion to carbon burial, *Global Biogeochem. Cycles*, *12*(2), 231–257, doi:10.1029/98GB00741.
Trimble, S. W. (1974), *Man-Induced Soil Erosion on the Southern Piedmont*, pp. 1700–1970, Soil Conserv. Soc. Am., Ankeny, Iowa.
Tucker, G. E., S. T. Lancaster, N. M. Gasparini, and R. L. Bras (2001a), The Channel Hillslope Integrated Landscape Development (CHILD) model, in *Landscape Erosion and Sedimentation Modeling*, edited by R. S. Harmon and W. W. Doe III, pp. 349–388, Kluwer Academic/Plenum Publishers, New York.
Tucker, G. E., S. T. Lancaster, N. M. Gasparini, R. L. Bras, and S. M. Rybarczyk (2001b), An object-oriented framework for distributed hydrologic and geomorphic modeling using triangulated irregular networks, *Comput. Geosci.*, *27*(8), 959–973, doi:10.1016/S0098-3004(00)00134-5.
USDA (1951), Soil survey manual, *U.S. Dep. Agric. Handbook*.
Van Oost, K., G. Govers, T. A. Quine, G. Heckrath, J. E. Olesen, S. De Gryze, and R. Merckx (2005), Landscape-scale modeling of carbon cycling under the impact of soil redistribution: The role of tillage erosion, *Global Biogeochem. Cycles*, *19*, GB4014, doi:10.1029/2005GB002471.
Van Oost, K., et al. (2007), The impact of agricultural soil erosion on the global carbon cycle, *Science*, *318*(5850), 626–629, doi:10.1126/science.1145724.
Van Oost, K., G. Verstraeten, S. Doetterl, B. Notebaert, F. Wiaux, N. Broothaerts, and J. Six (2012), Legacy of human-induced C erosion and burial on soil–atmosphere C exchange, *Proc. Natl. Acad. Sci.*, *109*(47), 19,492–19,497, doi:10.1073/pnas.1211162109.
Vivoni, E. R., V. Y. Ivanov, R. L. Bras, and D. Entekhabi (2004), Generation of triangulated irregular networks based on hydrological similarity, *J. Hydrol. Eng.*, *9*, 288–302, doi:10.1061/(ASCE)1084-0699(2004)9:4(288).
Yalin, M. S. (1977), *Mechanics of Sediment Transport*, Pergamon Press, Tarrytown, New York.
Yoo, K., R. Amundson, A. M. Heimsath, and W. E. Dietrich (2005), Erosion of upland hillslope soil organic carbon: Coupling field measurements with a sediment transport model, *Global Biogeochem. Cycles*, *19*, GB3003, doi:10.1029/2004GB002271.
Yoo, K., R. Amundson, A. M. Heimsath, and W. E. Dietrich (2006), Spatial patterns of soil organic carbon on hillslopes: Integrating geomorphic processes and the biological C cycle, *Geoderma*, *130*(1–2), 47–65, doi:10.1016/j.geoderma.2005.01.008.